MOF-Derived Chalcogenides Multifunctional Heterostructure Materials for High-Performance Supercapacitor and Oxygen Evolution Reaction Catalytic Activity

Muhammad Nasir Hussain[a]*, Nesrin Bugday[a], Stephen G. Hickey[b], Umair Shamraiz[c], Christopher A. Howard[d], Xiaobo Ji[e] and Sedat Yaşar[a]*

[a] İnönü University, Faculty of Science and Art, Department of Chemistry, 44280, Malatya, Türkiye.

[b]School of Chemistry and Biosciences, University of Bradford, BD7 1DP, United Kingdom.

[c]Department of Chemistry, Quaid-i-Azam University, Islamabad, 45320, Pakistan.

[d]Department of Physics & Astronomy, University College London, London WC1E 6BT, U.K.

[e]Deanship of Scientific Research, Imam Mohammad Ibn Saud Islamic University (IMSIU), Riyadh, Saudi Arabia.

[f]Central South University, College of Chemistry and Chemical Engineering, 410083, Changsha, China.

*Corresponding author, Muhammad Nasir Hussain, e-mail: nasir.hussain@inonu.edu.tr

Sedat Yaşar, e-mail: sedat.yasar@inonu.edu.tr

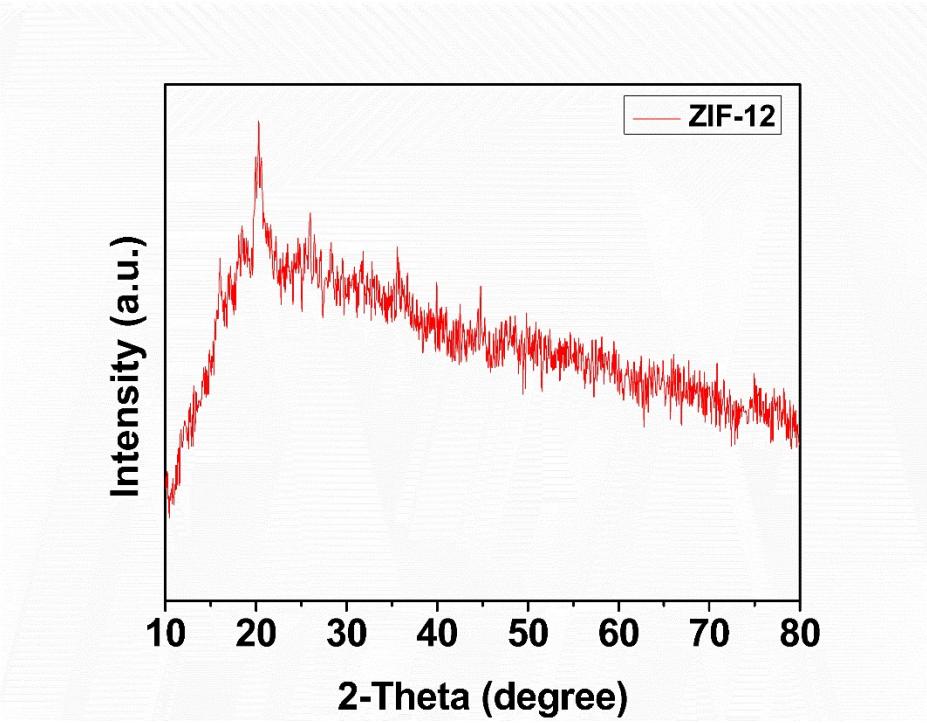

Figure S1. XRD pattern of ZIF-12.

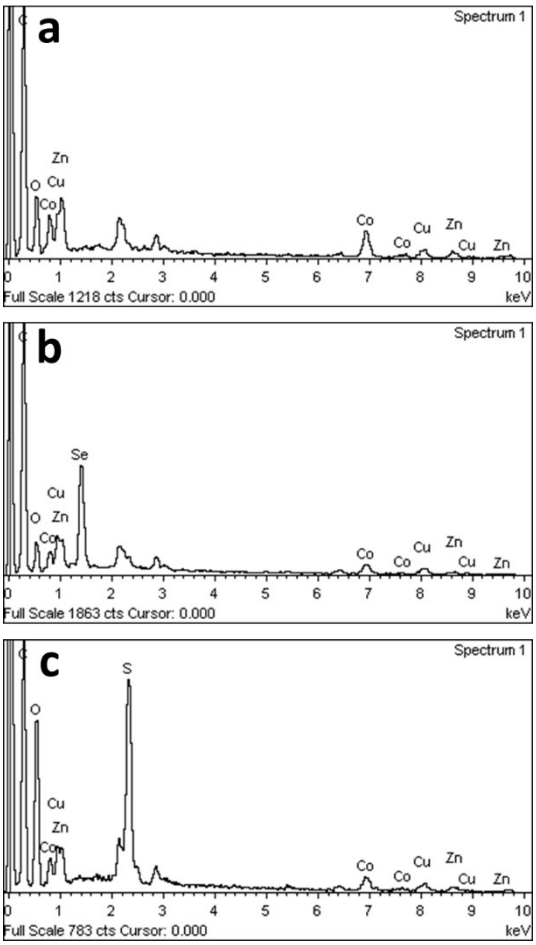

Figure S2. a) EDX spectrum of Cu/Zn/Co@NPC, b) $Cu_2Se/ZnSe/CoSe_2$@NPC, and c) $Cu_2S/ZnS/CoS_2$@NPC heterostructures.

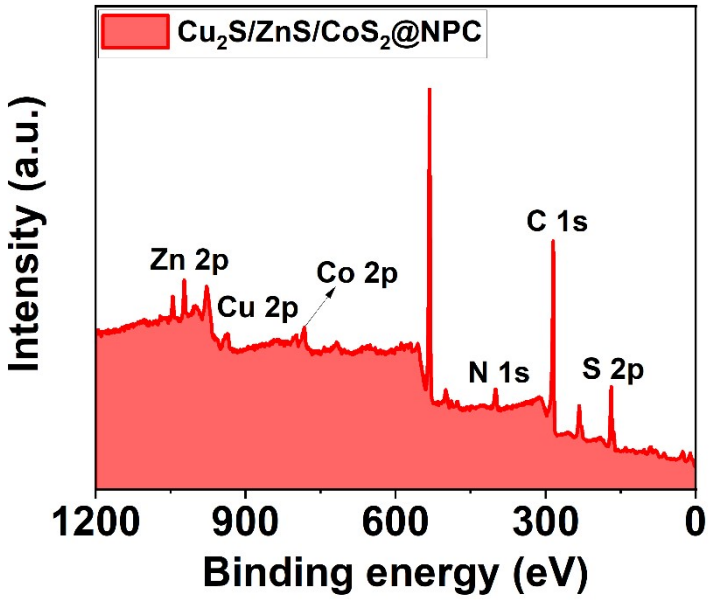

Figure S3. Survey spectrum of MOF-derived $Cu_2S/ZnS/CoS_2$@NPC heterostructure.

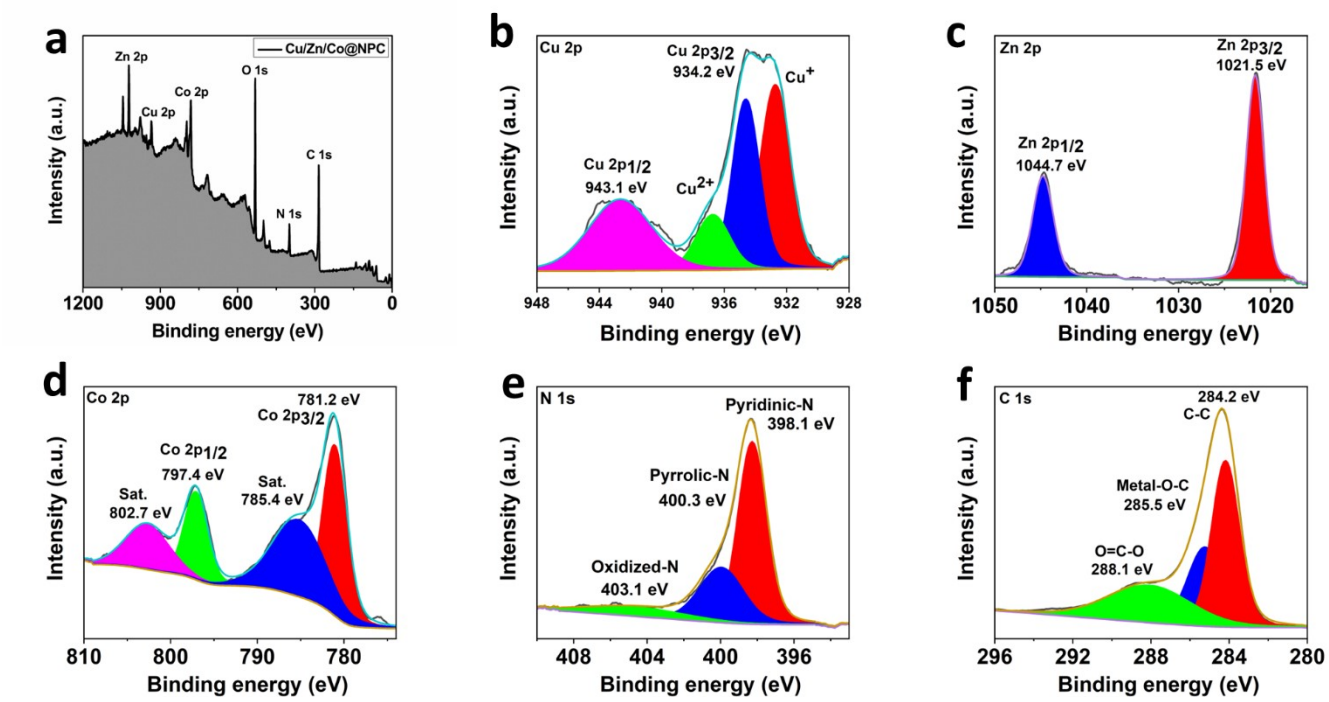

Figure S4. XPS analysis of MOF-derived Cu/Zn/Co@NPC heterostructure: a) Survey scan, b) Cu 2p, c) Zn 2p, d) Co 2p, e) N 1s, f) C 1s.

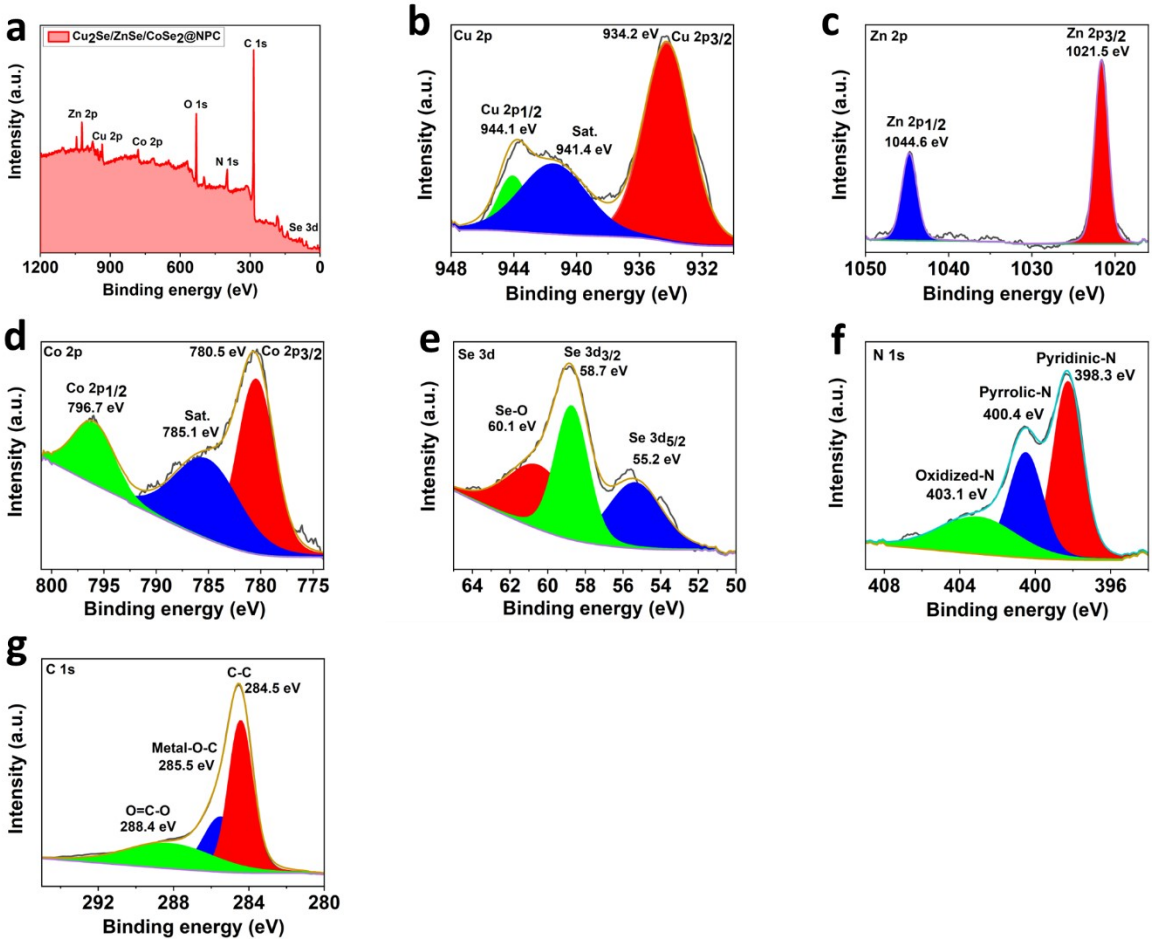

Figure S5. XPS analysis of MOF-derived $Cu_2Se/ZnSe/CoSe_2$@NPC heterostructure: a) Survey scan, b) Cu 2p, c) Zn 2p, d) Co 2p, e) Se 3d, f) N 1s, g) C 1s.

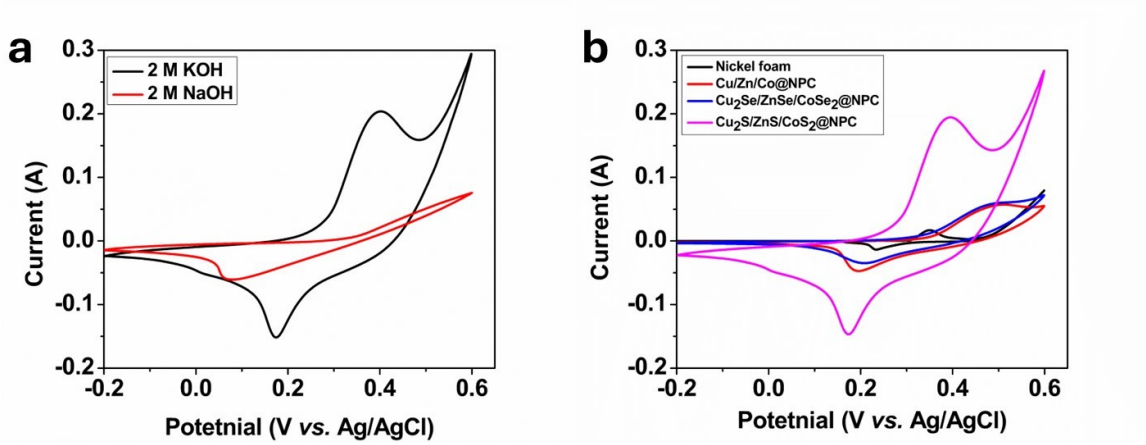

Figure S6. a) CV profiles of $Cu_2S/ZnS/CoS_2$@NPC heterostructure in 2 M NaOH and 2 M KOH, b) Comparative CV profiles of Cu/Zn/Co@NPC, $Cu_2Se/ZnSe/CoSe_2$@NPC, and $Cu_2S/ZnS/CoS_2$@NPC heterostructures in 2 M KOH at a scan rate of 10 mV s^{-1}.

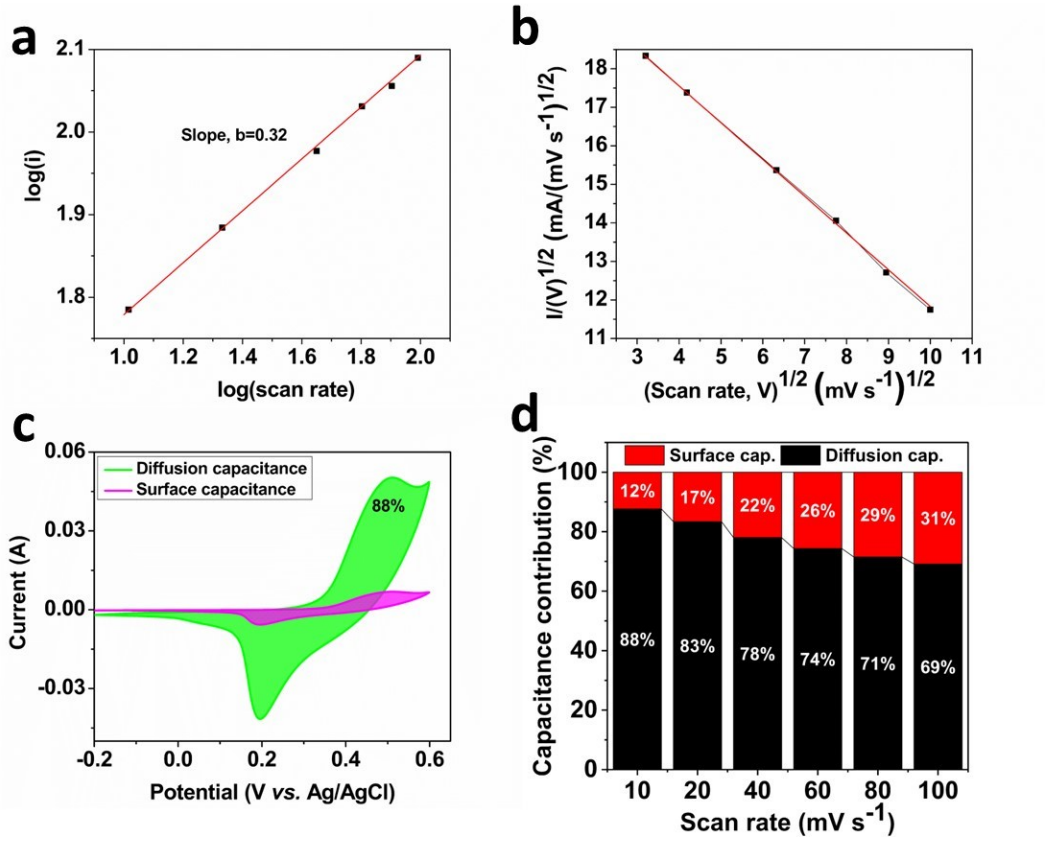

Figure S7. Dunn's method for quantitative analysis to evaluate surface and diffusion capacitance of Cu/Zn/Co@NPC: a) Plots of log(i) *vs.* log(v), b) Plots of ($i/v^{1/2}$) *vs.* ($v^{1/2}$), c) Contribution from surface and diffusion capacitance at 10 mV s^{-1}, d) Bar plots for the representation of surface and diffusion capacitive contribution at different scan rates.

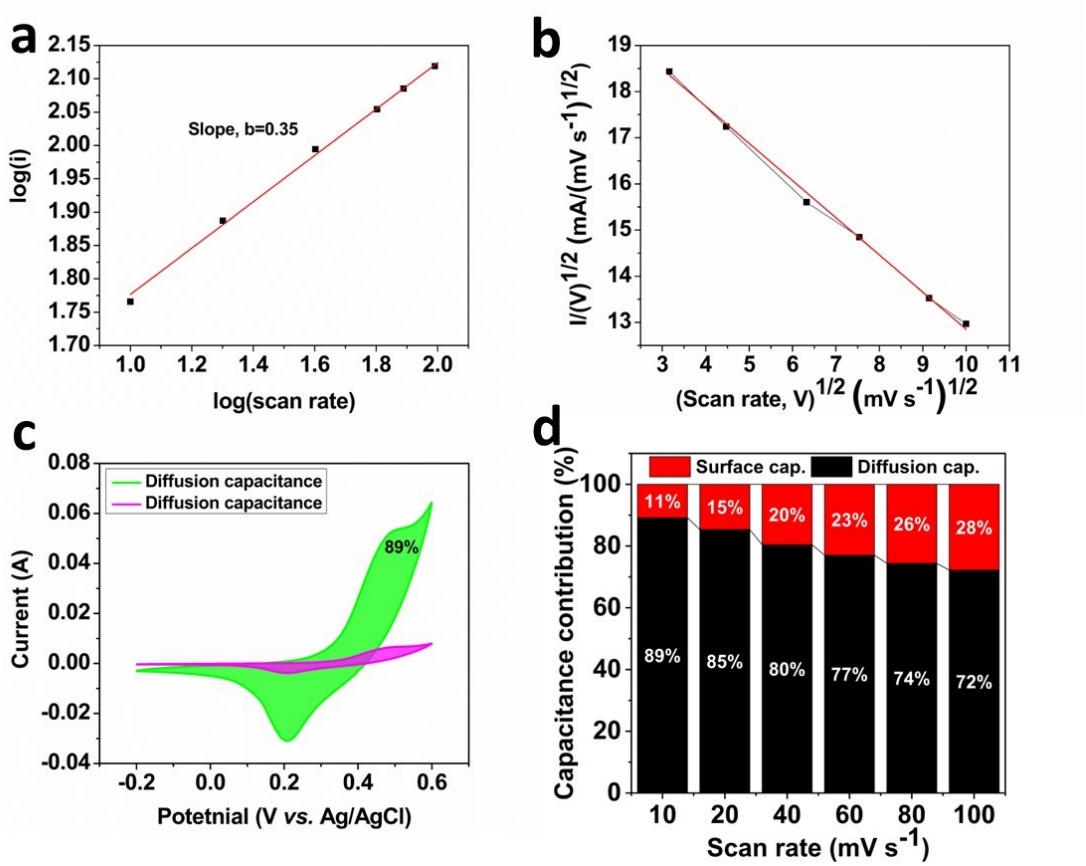

Figure S8. Dunn's method for quantitative analysis to evaluate surface and diffusion capacitance of $Cu_2Se/ZnSe/CoSe_2$@NPC: a) Plots of log(i) *vs.* log(v), b) Plots of $(i/v^{1/2})$ *vs.* $(v^{1/2})$, c) Contribution from surface and diffusion capacitance at 10 mV s^{-1}, d) Bar plots for the representation of surface and diffusion capacitive contribution at different scan rates.

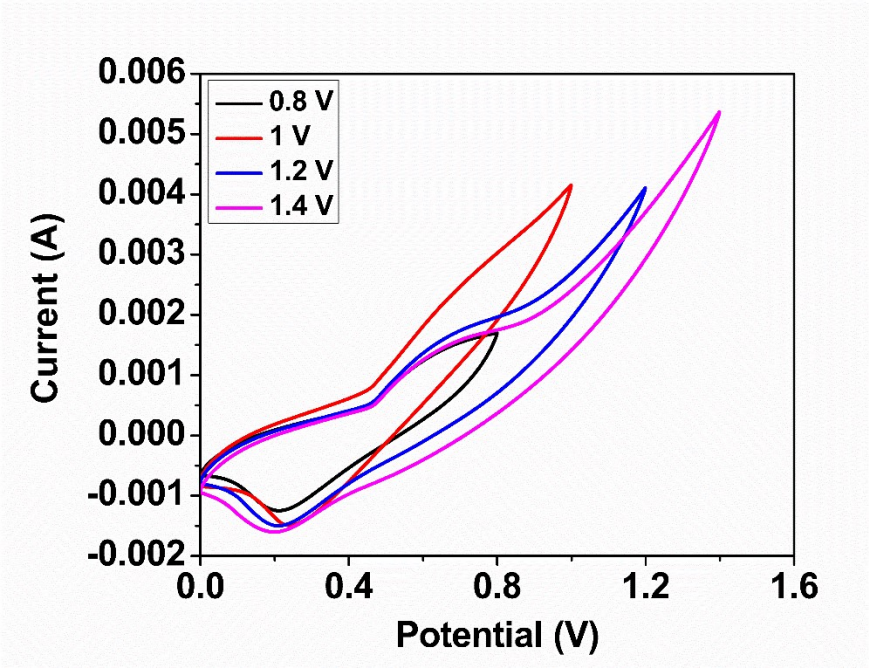

Figure S9. Potential window optimization of asymmetric device using $Cu_2S/ZnS/CoS_2$@NPC heterostructure.

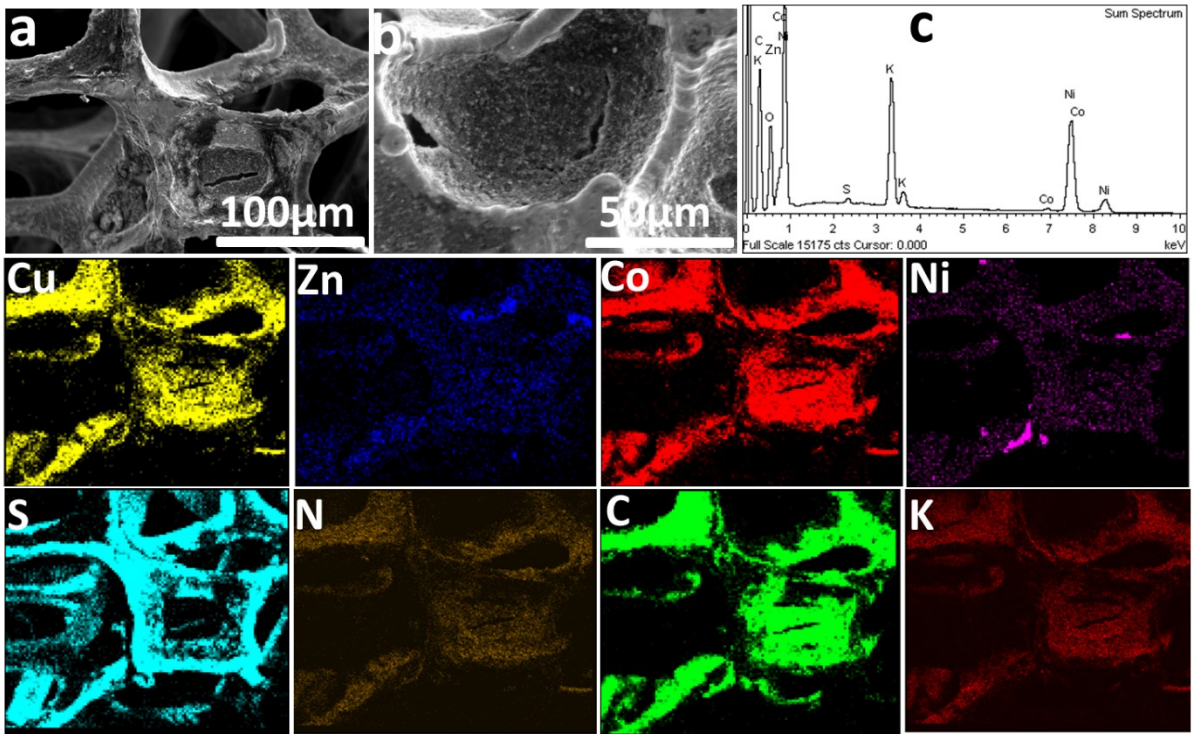

Figure S10. Post-electrochemical characterizations: a, b) SEM images deposited in nickel foam, b) EDX spectrum of $Cu_2S/ZnS/CoS_2$@NPC deposited in nickel foam and mapping images of each element in the sample.

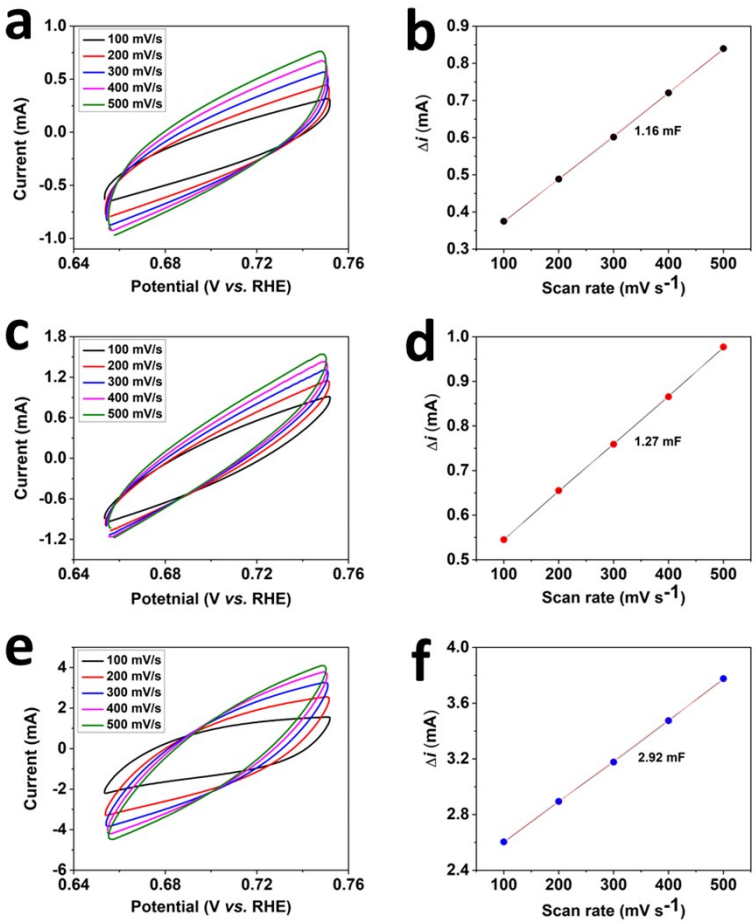

Figure S11. a, b, c) CV profiles of Cu/Zn/Co@NPC, $Cu_2Se/ZnSe/CoSe_2$@NPC, and $Cu_2S/ZnS/CoS_2$@NPC heterostructures at various scan rates in 1 M KOH, d, e, f) Linear fit curves of corresponding capacitive currents.

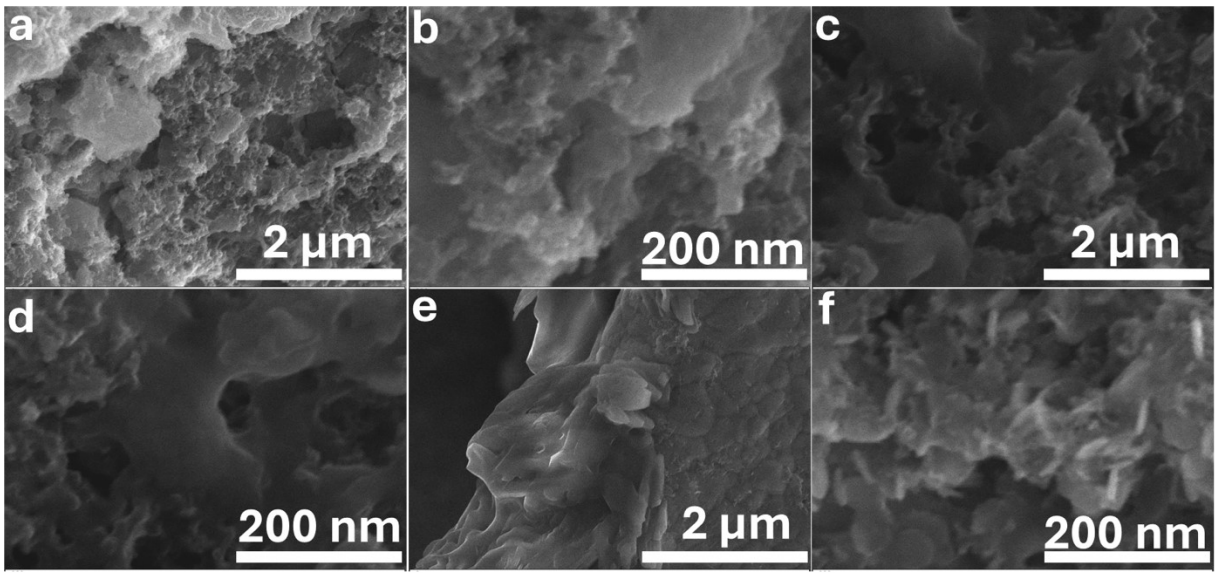

Figure S12. Post-OER SEM images: a, b) Cu/Zn/Co@NPC deposited in nickel foam at 2 µm and 200 nm, c, d) , $Cu_2Se/ZnSe/CoSe_2$@NPC deposited in nickel foam at 2 µm and 200 nm, and e, f) $Cu_2S/ZnS/CoS_2$@NPC deposited in nickel foam at 2 µm and 200 nm.

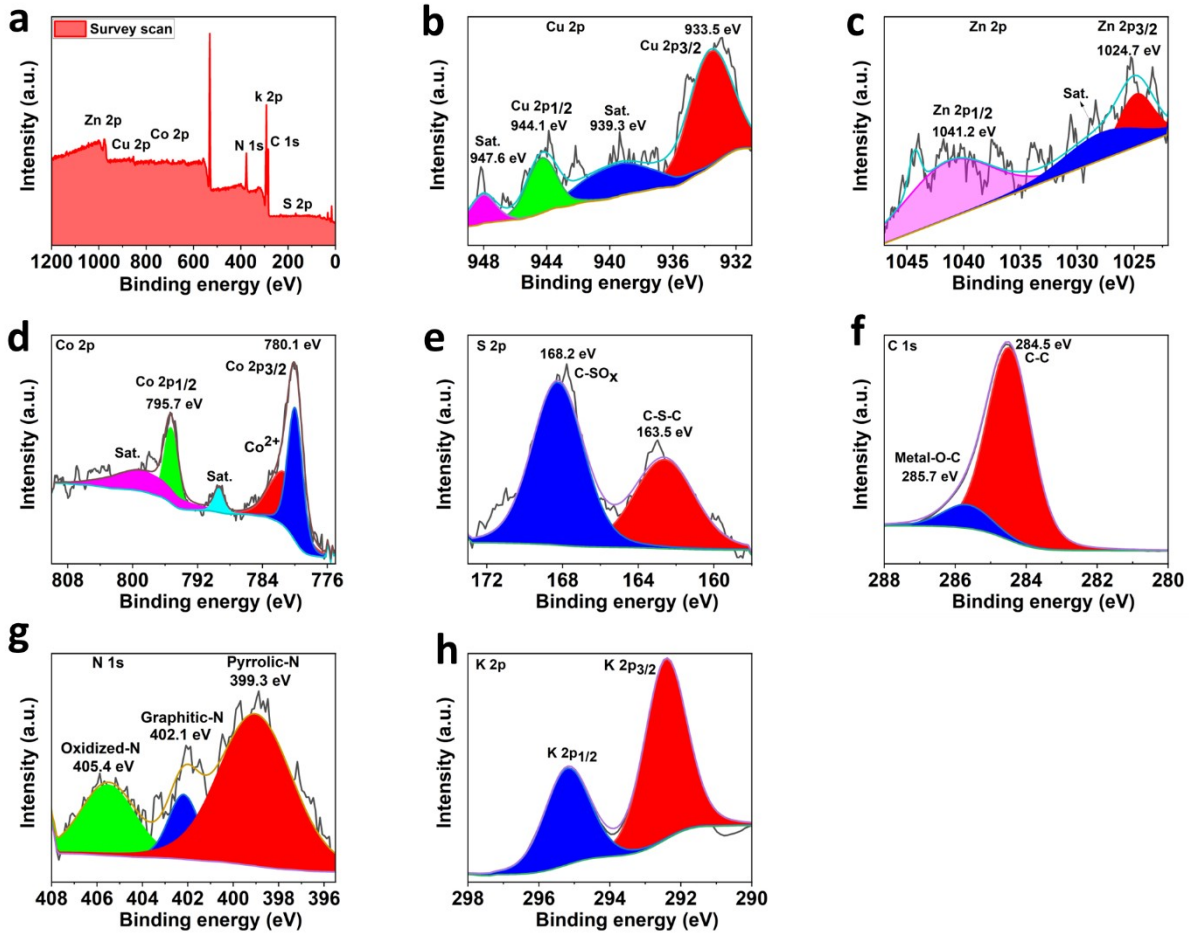

Figure S13. Post-OER XPS analysis of MOF-derived $Cu_2S/ZnS/CoS_2$@NPC heterostructure: a) Survey scan, b) Cu 2p, c) Zn 2p, d) Co 2p, e) S 2p, f) C 1s, g) N 1s, and h) k 2p.

Table S1. EIS parameters obtained after model circuiting fitted.

Parameters	**Values**	**Pct. Error (%)**
R_s (ohm)	2.373	4.809
R_{ct} (ohm)	66.59	8.564
CPE, Y_o, (S·s^n)	0.0001232	15.69
Warburg, Y_o, (S·s^.5)	0.004463	31.95
Chi-squared	0.00545	-

Table S2. OER performance comparison with reported MOF-derived materials.

Catalyst Material	**Electrolyte**	**Overpotential (η @10 mA cm^{-2})**	**Tafel slope (mV dec^{-1})**	**Stability**	**Ref.**
MOF-derived FeNiZnS	1 M KOH	249 mV	41.4	60 h	[1]
MOF-derived MoCoNiS	1 M KOH	151 MV	44.7	10 h	[2]
MOF-derived Fe@$CoMo_2S_4/Ni_3S_2$	1 M KOH	167 mV	13.77	100 h	[3]
MOF-derived FeCoMnMo/NF-C-S	1 M KOH	174 mV	66.3	120 h	[4]
Cu-Co-S@Cu-MOF/CF	1 M KOH	136 mV	64	100 h	[5]
RuO_2	1 M KOH	146 mV	152.8	-	[5]
MOF-derived CoS@C supported MXene	1 M KOH	257 mV	95	12 h	[6]
RuO_2	1 M KOH	331 mV	139	-	[6]
MOF-derived S/CuCoPSe@C	1 M KOH	360 mV	116	48 h	[7]
RuO_2	1 M KOH	280 mV	105	-	[7]
rGO/IrO_2/TiO_2	1 M KOH	240 mV	53.81	50	[8]
MOF-derived $Cu_2S/ZnS/CoS_2$@NPC	**1 M KOH**	**120 mA**	**92**	**30 h**	**This work**

Tafel Slope Derivation

The Tafel slope is derived from the Butler-Volmer equation, which describes the relationship between current density and overpotential in electrochemical reactions.

The Butler-Volmer equation is:

$$i = i_0 [e^{\frac{\alpha n F \eta}{RT}} - e^{-\frac{(1-\alpha) n F \eta}{RT}}]$$

At high overpotential, one exponential term becomes negligible. For an anodic reaction (such as OER), the equation simplifies to:

$$i \approx i_0 e^{\frac{\alpha n F \eta}{RT}}$$

Taking the logarithm of both sides:

$$log i = log i_0 + \frac{\alpha n F}{2.303 RT} \eta$$

Rearranging gives the **Tafel equation**:

$$\eta = log i_0 + \frac{\alpha n F}{2.303 RT} \eta$$

here

- η= overpotential
- i= current density
- a= intercept
- b= Tafel slope

The Tafel slope (b) is:

$$b = \frac{2.303 RT}{\alpha n F}$$

At 25 °C (298 K) this becomes approximately:

$$b = \frac{0.059}{\alpha n} V\ dec^{-1}$$

Thus, the Tafel slope reflects the reaction kinetics and charge-transfer mechanism of the electrocatalytic process.

References

1. T. Liu, Y. Zhang, J. Yu, M. Hu, Z. Wu, X. Wei, S. Yu and Y. Du, *Inorg. Chem. Front.,* 2024, **11,** 6064-6071.
2. J.-F. Qin, M. Yang, T.-S. Chen, B. Dong, S. Hou, X. Ma, Y.-N. Zhou, X.-L. Yang, J. Nan and Y.-M. Chai, *Int. J. Hydrogen Energy.,* 2020, **45,** 2745-2753.
3. S. Yu, D. Liu, C. Wang, J. Li, R. Yu, Y. Wang, J. Yin, X. Wang and Y. Du, *J. Colloid Interface Sci.,* 2024, **653,** 1464-1477.
4. Y.-Y. Chen, S. Kubendhiran, S. Perumal, P.-Y. Lee, S.-N. Lin, W.-Y. Yu, L.-Y. Lin and K.-C. Ho, *Mater. Today Energy.,* 2026, **57,** 102226.
5. B. Li, Y. Sun, Y. Zhang, W. Jiang, J. Lang, G. Che, C. Liu and Y. Wu, *Small.,* 2025, **21,** e10545.
6. K. Farooq, M. Murtaza, Z. Yang, A. Waseem, Y. Zhu and Y. Xia, *Nanoscale Adv.,* 2024, **6,** 3169-3180.
7. M. Maniyazagan, E. Shanmugasundaram, P. Naveenkumar, K. P. Nithyanandam, H.-W. Yang, S. Thambusamy and S.-J. Kim, *J. Power Sources.,* 2025, **647,** 237379.
8. S. Luo, Z. Zuo and H. Sun, *Molecules.,* 2025, **30,** 2069.